

Yearly Progress Report (June 2019):
Award Number: DE-SC0018359
Title: Simulation of Fission Gas in Uranium Oxide Nuclear Fuel

Lead PI: Anders D. Andersson, Los Alamos National Laboratory
 UTK Institutional PI: Brian Wirth, UTK-ORNL Governor’s Chair Professor of Computational Nuclear Engineering

<i>Institution</i>	<i>Principal Investigator</i>	<i>Senior Personnel</i>
ANL	Barry Smith	
INL	Giovanni Pastore	Cody Permann, Derek Gaston, Daniel Schwen
LANL	Anders Andersson	Blas Uberuaga, Danny Perez, Tom Swinburne
ORNL	David Bernholdt	Phil Roth
SNL	Habib Najm	Khachik Sargsyan
UF	Michael Tonks	Dong-Uk Kim, Ali Muntaha
UTK	Brian Wirth	Abdullah Al-Fadhili, Sophie Blondel

The behavior of xenon (Xe) in nuclear fuel is of critical importance to nuclear fuel performance, because the diffusion and precipitation of Xe in fission gas bubbles influences both the amount of fuel swelling and the quantity of fission gas released to the fuel rod plenum [1]. Despite decades of investigation, significant uncertainties exist regarding the underlying mechanisms controlling Xe diffusion, precipitation and release that impact predictions of fission gas swelling and release during both normal operation and transient conditions in accidents. Such uncertainties limit the accuracy of integrated fuel performance models [2], which are important to many DOE Office of Nuclear Engineering programs including the Nuclear Engineering Advanced Modeling and Simulation (NEAMS) and the Consortium for the Advanced Simulation of Light water reactors (CASL). Most fission gas behavior models used for fuel performance calculations trace back to the 1957 formulation by Booth [3], the mid-to-late 1960’s formulation by Speight and co-workers [4,5]; or the slightly more recent work by Turnbull [6], White and Tucker [7], and Forsberg and Massih [8,9]. These models typically rely on a small number of spatially independent partial differential equations, or even a single partial differential equation, along with the concept of an effective diffusivity to account for the effect of intra-granular fission gas bubbles on the bulk diffusion rate [4]. These models are clearly over-simplifications of the actual behavior of noble gas within the fuel. Indeed, the dynamics of fission gas bubbles, which form both within the grains (intra-granular) and on grain boundaries (inter-granular), affects the rate of fission gas diffusion and release, and also determines the fission gas swelling [1,7,10]. Despite being a key determinant of fission gas effects, which control fuel performance, accurate physically based models of intra-granular bubble evolution are still lacking in current models. Rather, the characteristics of the bubble population (number density, mean size) are given as constant parameters or calculated through simplistic, empirically based functions of temperature [2,7,8].

Concomitant to intra-granular gas bubble evolution is intra-granular gas atom diffusion, which leads to gas accumulation at grain boundaries leading to the formation of inter-granular fission gas bubbles. Grain boundaries are structurally and energetically different from the interior of grains, providing dramatic differences in the diffusion rates of fission gases and vacancies, and serving as regions for nucleation and growth of fission gas bubbles typically of the size of one to a few microns. Grain boundary bubbles account for the majority of fuel gaseous swelling for normal reactor operating conditions and moderate burnups below about 45 GWd/tU – whereas swelling associated with coarsened intra-granular bubbles

can become dominant at high burnup and during power transients to high temperatures [11,12]. Moreover, the formation and growth of fission gas bubbles on grain boundaries is primarily responsible for fission gas release, which occurs by the interlinking of these bubbles and the associated formation of pathways to the exterior or fracture surfaces.

As the complex bubble evolution process strongly depends on the specific fuel irradiation conditions and reactor operating history [10-14], this gap in current modeling capability significantly limits the accuracy and transferability of available treatments. Therefore, developing effective modeling capabilities for fission gas bubble evolution is a key issue in achieving higher standards of accuracy for predictions of fission gas swelling and release in fuel performance analysis.

The objective of this project is to advance the mechanistic understanding of fission gas behavior in UO_2 nuclear fuel by developing a mesoscale fission gas simulator that takes advantage of leadership class computers. This will enable an accurate and physically based fission gas release model for application in integrated fuel performance codes. The model will be informed by results from large-scale atomistic and mesoscale simulations of the three stages of fission gas release, including diffusion and intra-granular bubble formation, bubble growth and coalescence on grain faces, and the transport of gas through interconnected grain edge tunnels to the fuel rod plenum. In order to address this complex problem, existing atomistic and mesoscale simulation tools will be further developed to take advantage of DOE high performance computing capabilities. The simulation tools will undergo rigorous uncertainty quantification and validation. In addition to gas release and retention, the integrated tool will predict their impact on performance parameters such as fuel swelling and thermal conductivity.

Our project involves developing an advanced mechanistic model of fission gas release in oxide nuclear reactor fuel that consider all three stages of gas release and explicitly includes the impact of both intra- and inter-granular gas bubbles. The development of this model will use the insights from molecular dynamics (MD) simulations with accelerated MD techniques (AMD) and selected density functional theory (DFT) calculations to provide quantitative assessments of fission gas diffusion. The behavior of the intra-granular bubbles will be investigated using cluster dynamics. We will rely on a hybrid, and spatially-dependent, continuum model, containing discrete cluster dynamics for clusters of size up to a few hundred gas atoms and a grouping scheme bundling a range of cluster sizes into distributions for capturing larger clusters. The inter-granular bubble behavior will be investigated using the phase field method (PFM) by enhancing the numerical performance of the MARMOT phase field code used to solve the problem. Both the cluster dynamics and phase field simulations will be deployed on DOE HPC systems. The cluster dynamics code focusing on intra-granular fission gas behavior will be coupled to phase field simulations by providing the flux of gas atoms to the grain boundaries. Our project also involves the use of uncertainty quantification across the simulation length and timescales, and will validate predictions against existing and emerging data on fission gas bubble distribution in nuclear fuel. As well, the uncertainty of the final fission gas release model will be quantified and compared against the uncertainty of the existing data to ensure that our development efforts have significantly decreased the uncertainty and increased the accuracy of the engineering-scale fission gas release model.

The outcome of this project will be improved insight into the atomistic processes of Xe diffusion and clustering, and the validation of a leadership class fission gas simulator, Xolotl-fission, for modeling the spatially dependent, and multi-modal intragranular bubble population evolution within nuclear fuel. Further, the Xolotl-fission code will be coupled to the mesoscale MARMOT phase field model to provide a self-consistent, high fidelity modeling approach for both intragranular and intergranular fission gas bubbles, leading to an improved physical model of fission gas release. These outcomes will set the stage for future multiscale model research activities, coupled to a comprehensive uncertainty quantification analysis, to ultimately treat fission gas swelling and release as inherently coupled to bubble evolution. Such advances are crucially needed to deliver improved, physics-based models needed by advanced,

engineering-scale fuel performance models under development within the DOE NE programs, namely the CASL and NEAMS.

In order to accomplish these goals, the research is organized in three thrusts with defined interfaces between them:

Thrust 1: DFT and long-time scale atomistic simulations to understand fission gas and defect behavior. Fission gas diffusion is enabled by uranium and oxygen vacancies. We are using molecular dynamics (MD) and in particular accelerated molecular dynamics (AMD) techniques to directly simulate the kinetic behavior of large Xe-vacancy clusters and their interactions with other defects. The MD and AMD simulations are complemented by selected DFT calculations. These properties are critical for an accurate mesoscale description of fission gas evolution. The thermodynamic and kinetic properties of fission gas atoms at grain boundaries and dislocations will also be probed by MD and AMD methods in order to provide data for the phase field model of inter-granular bubbles.

Thrust 2: Spatially discretized cluster dynamics and MARMOT phase field simulations to understand fission gas bubble behavior. This task involves two continuum approaches tailored to describe 1) nucleation, growth and re-resolution of intra-granular bubbles and 2) growth and coalescence of inter-granular bubbles on grain faces and edges. The first approach is a hybrid and spatially dependent continuum model, called Xolotl-fission, consisting of spatially-discretized, 3D reaction-diffusion cluster dynamics coupled to a methodology to treat the larger size bubble population evolution to model strongly bi- (or, in some cases multi-) modal bubble size distributions. The two methods will be coupled as Xolotl-fission will provide fluxes of gas atoms to grain boundaries to a phase field model (the second approach), as implemented in the mesoscale MARMOT code to capture the growth and interconnection of grain face bubbles and how they interact with grain edges to form tunnels that allow gas atoms to vent to free surfaces in massive 3D polycrystal simulations. MARMOT developers working with ASCR funded scientists are improving the computational efficiency of MARMOT to facilitate these 3D microstructures requiring leadership class computational resources. Both Xolotl-fission and MARMOT will be used to improve the understanding of fission gas behavior and release, and support development of a reduced order fission gas release model for application to the BISON fuel performance code.

Thrust 3: Uncertainty quantification and experimental validation. Global sensitivity analysis is used to identify important fission gas diffusion mechanisms. These will be applied to both the Xolotl-fission and MARMOT as well as to the coupled version of the codes, to assess the impact of specific gas diffusion mechanisms on intra-granular bubble evolution, and subsequently inter-granular bubble evolution and fission gas release. We will also apply Bayesian inference methods for statistical calibration of fission gas diffusion models with embedded model error representations, arriving at probabilistic representations of relevant uncertain model parameters. These will subsequently be used in Xolotl-fission and MARMOT computations, providing predictions of fission gas bubble populations and diffusion coefficients with quantified uncertainty. Available data will be used to assess confidence in the underlying models, via Bayesian model evidence estimation, thereby providing means for model validation, hypothesis testing and model selection. Experimental validation will particularly emphasize validation against experimental work on the continuum (microstructure) and engineering scales.

This document describes the project progress in the second year, from approximately June 2018 – May 2019. Our most significant outcomes have involved development of the coupling framework for Xolotl and MARMOT, continued performance improvements in Xolotl, uncertainty quantification analysis of the free energy cluster dynamics and Xolotl codes, new engineering scale model for intra-granular bubble evolution during transients, and to finalize the Xe diffusion model based on extended vacancy clusters. The remainder of this document describes the progress within each thrust, and incorporates computer science and applied mathematics research activities as appropriate.

PROGRESS ON PROJECT RESEARCH ACTIVITIES

Thrust 1: DFT and long-time scale atomistic simulations to understand fission gas and defect behavior

The two main tasks over the past year have been to 1) finalize the Xe diffusion model based on extended vacancy clusters, and 2) apply molecular dynamics (MD) and accelerated molecular dynamics (AMD) simulations to formation and migration of combined uranium and oxygen interstitial clusters. The first task included resolving a few remaining data gaps with new density functional theory (DFT) and molecular statics (MS) calculations as well as finishing and documenting the free energy cluster dynamics (FECD) code. This code is implemented under the MOOSE/MARMOT framework and simulates interactions between point defects and Xe atoms, which controls the diffusivity under irradiation. Note that FECD treats much smaller clusters and includes higher “chemical resolution” than the Xolotl code, which aims at simulating bubble formation, growth and resolution by including cluster sizes well above 100000 atoms compared to the <100 atoms treated by FECD. A significant portion of the FECD development was devoted to making the code available and usable to the UQ thrust personnel working on quantifying model sensitivity and uncertainty. The results of the DFT/MS work have been published in one journal paper [15], with another under review for the FECD methodology [16] and a third study of Xe diffusion under irradiation being prepared for submission [17]. The second task on interstitial clustering and diffusion was pursued as an important physics mechanism contributing to point defect and Xe evolution under irradiation in UO_2 and as a testbed for application of large-scale AMD simulations.

DFT and cluster dynamics simulations of Xe-vacancy interactions and diffusion in UO_2

The properties of individual point defects, clusters thereof and interaction with Xe atoms under thermal equilibrium conditions were studied using a combination of DFT and MS calculation combined with a point defect model for predicting diffusion rates. This study was published in [15] and the key results are summarized in Figure 1, which shows that, under thermal equilibrium or intrinsic conditions, Xe diffusion

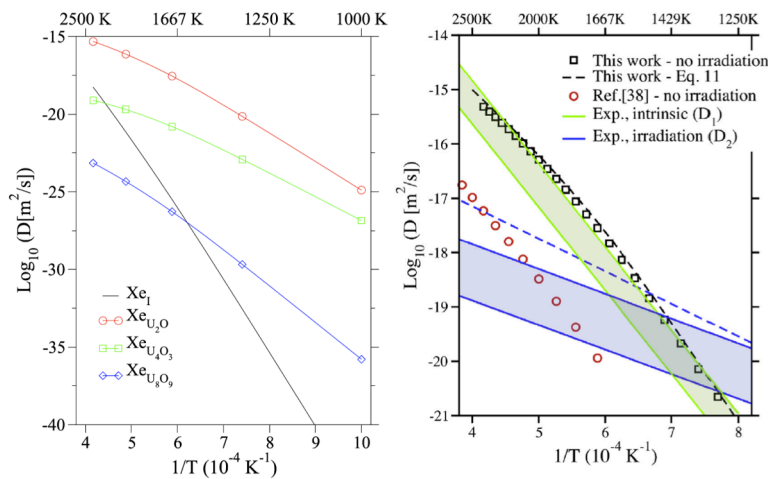


Figure 1. a) The Xe diffusion rate for the clusters with the highest diffusivity and for Xe interstitials under thermal equilibrium conditions in UO_2 . b) Total Xe diffusivity in UO_2 , compared to previous calculations and experimental results. The plots are reproduced from [15].

occurs by the $\text{Xe}_{\text{U}_2\text{O}}$ cluster, migrating via a vacancy mechanism, across the full temperature range. The extended Xe-vacancy clusters hypothesized to be important under irradiation have too low concentrations to be of any significance under thermal equilibrium conditions. However, their concentrations and resulting diffusivities are sufficiently close to the dominant $\text{Xe}_{\text{U}_2\text{O}}$ mechanism that they may be important under irradiation due to an increased concentration of uranium vacancies, see below. Even though our diffusion prediction is at the high end of the experimental range, the agreement is considered good.

The FECD code, which is implemented under the MOOSE/MARMOT framework and internally given the FECD name for convenience, was developed to investigate the behavior of small clusters of point defects and Xe in irradiated UO_2 ,

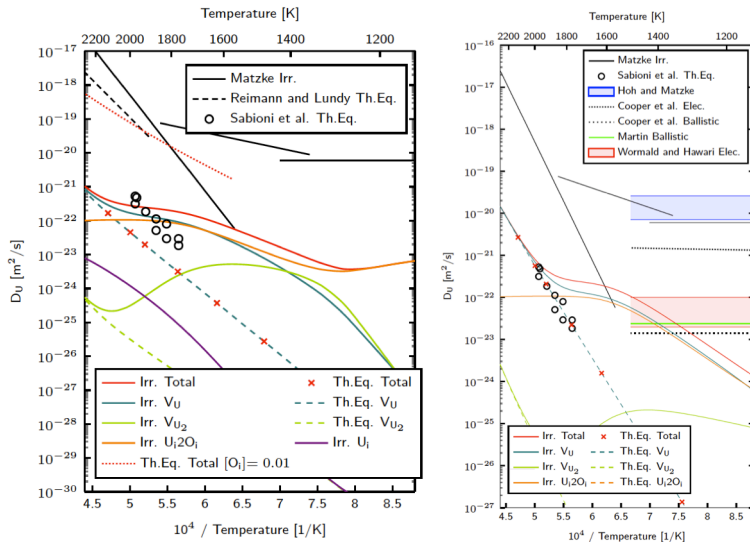


Figure 2. a) Calculated values for uranium self-diffusion plotted as solid lines for irradiation enhanced values, and dashed lines for thermal equilibrium values. In addition, the total thermal equilibrium self-diffusion when $x = [\text{O}_i] = 0.01$ is enforced is plotted. b) Calculated values of uranium self-diffusion under irradiation and at thermal equilibrium with slight data modifications to better fit the experimental results. Calculated values of athermal diffusion are provided for comparison as well. The figures are reproduced from [16].

based on input from DFT and empirical potential calculations. The FECD methodology was described in a journal paper that is currently under review [16] and, in that paper, it was also tested for uranium self-diffusion under irradiation. The key results for uranium self-diffusion are summarized in Figure 2. Even though diffusion occurs by uranium vacancies under thermal equilibrium conditions, as expected, under irradiation below $\sim 1600\text{K}$, diffusion by the U_i2O_i cluster (one uranium interstitial with two additional bound oxygen interstitials, i.e. an anti-Schottky defect) is predicted to be competitive. This is due to the low migration barrier of the cluster, which is enabled by the recently identified mechanism shown in Figure 3. Most notably

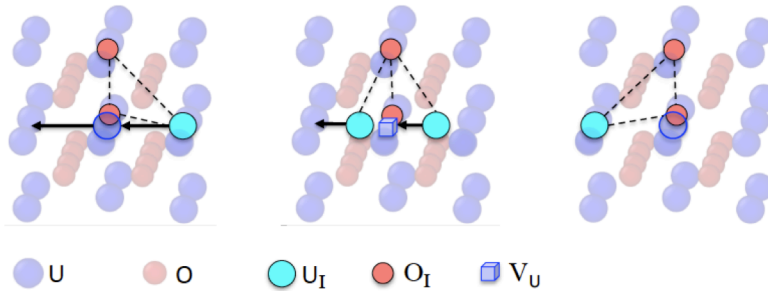


Figure 3. The interstitialcy diffusion mechanism of an U_i2O_i anti-Schottky cluster, progressing from left to right: the initial state with the interstitial uranium ion shown in turquoise and the interstitial oxygen ions in red (left); the saddle point, which is equidistant between the initial and final states (center); and the final state (right). The figure is reproduced from [16].

the barrier is less than half than that for the single uranium interstitial without the bound oxygen interstitials. We suspect that this mechanism and related mechanisms for even larger interstitial clusters may be of high importance. Therefore, these are further studied by MD and AMD simulations, as described in the next section. According to the final “best parameter set”, the vacancy mechanism still dominates, but with a surprisingly small margin. Agreement with experiments for uranium self-diffusion is good under thermal

equilibrium conditions, but significant deviations are observed for in-pile conditions. We hypothesize this to be a consequence of non-stoichiometry in the samples used for experimental measurements.

The rationale for developing the FECD code was to predict Xe diffusion under irradiation by mechanisms involving vacancies and interstitial defects. The application of FECD to this problem has almost been completed and the predicted rate of Xe diffusion is summarized in Figure 4. The main conclusions from

this figure are that, due to the high concentration of uranium vacancies induced by irradiation, the concentration of extended Xe-vacancy clusters increases rapidly with decreasing temperatures and at about 1650K the concentrations are high enough for the mobile Xe_{U4O3} cluster to overtake the Xe_{U2O} cluster diffusion mechanism. Comparison with experimental data indicates that this mechanism does a good job capturing the increase in diffusivity and change in slope observed in experiments due to irradiation. At even lower temperatures the predicted irradiation-enhanced diffusivity starts decreasing more rapidly than perhaps observed in experiments, which according to our prediction roughly coincides with diffusion by atomic mixing induced by thermal spikes surpassing the thermally activated mechanism. The good agreement with the Xe diffusivity in both

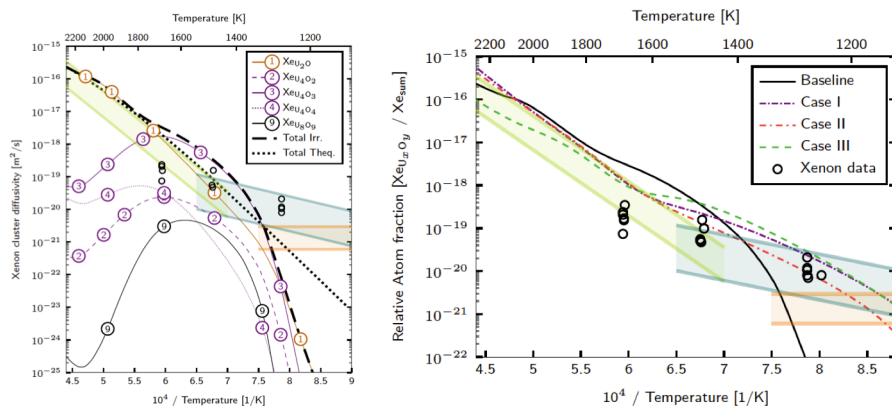


Figure 4. a) Xenon diffusivity for the baseline case under irradiation. The regimes proposed by Turnbull et al. [6] are included for reference. b) Xenon diffusivity for several different cases: Baseline, the best case for uranium self-diffusion from Case I from Matthews et al. [16,17], Case II (same as Case I with different T dependence for the partial pressure), and Case III (same as Case II with a different reference temperature for ideal UO_2 stoichiometry). The regimes proposed by Turnbull et al. [6] are included for reference.

the thermal and irradiation enhanced regimes is very encouraging and the results can be applied directly in the coupled Xolotl-MARMOT code to describe gas evolution and release of Xe gas under irradiation. The results can also be used directly in the Bison fuel performance code as replacement for the current (unperturbed) bulk diffusivity.

Empirical potential studies of small interstitial cluster aggregates in UO_2 under irradiation

We have already introduced the importance of the U_2O_i cluster above. We would like to study this diffusion mechanism in more detail using both standard MD and AMD simulations, with the intent of extending these studies to even larger clusters of interstitials. The latter study is motivated by indirect experimental evidence of a very fast mobility for uranium interstitials, which is not supported by any simulations for single uranium interstitials (without any coordinated oxygen interstitials), but perhaps possible to reconcile with anti-Schottky defects and even large interstitial clusters, which would eventually form irradiation induced dislocation loops. The latter are important as defect sinks. This problem is also a good testbed for new AMD methods developed under the NE-SciDAC project.

Two interatomic potentials are used to model the interstitial defects. One is the Morelon potential [18], which has been used before for modeling of interstitial dislocation loops. The other potential is the many-body model developed by Cooper, Rushton, and Grimes (CRG) [19]. The parallel replica dynamics (ParRep) method [20-22], as implemented in the LAMMPS code [23], is used for studying migration events at high temperatures. The ParRep method allows us to efficiently deploy the simulations on LANL's HPC cluster platforms. However, first, we tested the two potentials for the basic formation and migration properties of uranium interstitials with or without oxygen interstitials. The migration energies for the U_2O_i cluster are 2.3 eV in the CRG case, and 0.98 eV in the Morelon case, to be compared to the 1.97 eV from DFT. Both are substantially lower than the single U interstitial migration energies 3.1 eV (CRG) and 2.3 eV (Morelon), again in qualitative agreement with the 4.08 eV barrier obtained from DFT.

Next, we placed multiple UO_2 interstitial clusters in a $\{111\}$ plane of bulk UO_2 supercell to mimic the early stage growth of a circular $\langle 111 \rangle / 3$ dislocation Frank loop. Fig. 5(a) shows that the formation energies of the UO_2 interstitial clusters follow a monotonic decreasing trend with the cluster size (up to 69) for both empirical potentials. However, for the binding energies of these clusters (the averaged difference between total energies of cluster and the sum of isolated single clusters), there is substantial difference between the CRG potential and Morelon potential. The Morelon potential predicts a monotonic increasing trend as the cluster size becomes larger, while the CRG potential predicts non-monotonic behavior for cluster size of 2, 3, and 6.

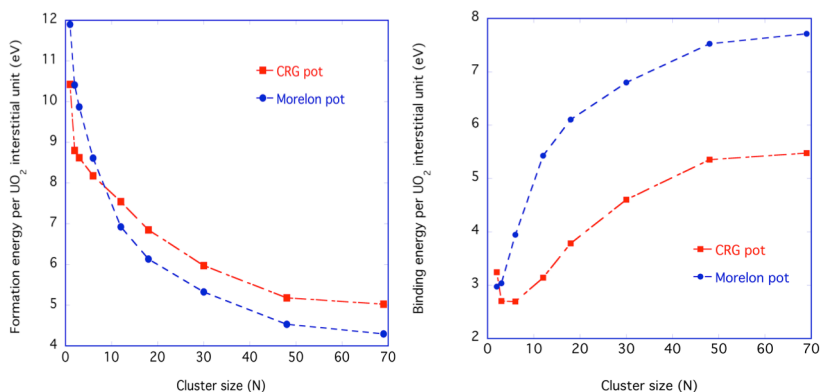


Figure 5. a) The formation and b) binding energies of UO_2 interstitial clusters.

The Morelon potential predicts a monotonic increasing trend as the cluster size becomes larger, while the CRG potential predicts non-monotonic behavior for cluster size of 2, 3, and 6.

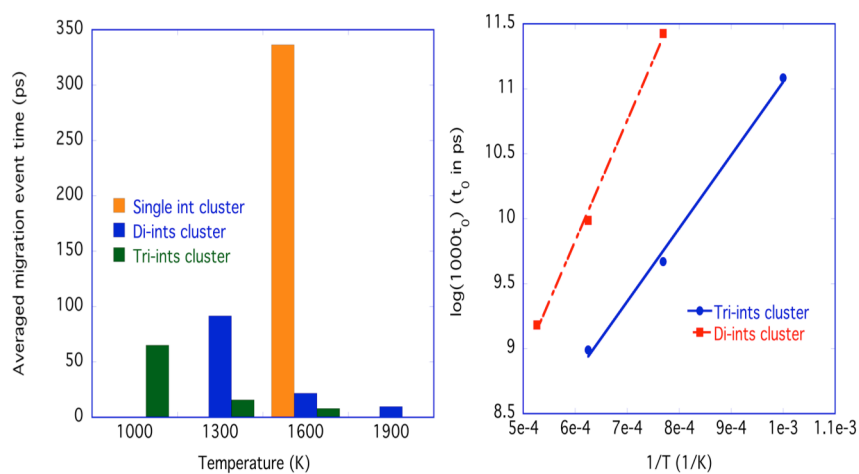


Figure 6. a) The averaged time for migration events during MD simulations at different temperatures for single, di-, and tri-interstitial clusters. b) An Arrhenius plot of the migration event time, directly related to the cluster diffusivities.

Clearly, both di- and tri-interstitial clusters use much less time in the MD simulations for migration events to take place. In Fig. 6b, the migration energies extracted from the simulations for di- and tri-interstitial cases are shown. The effective migration energies of 0.78 eV (di-interstitials) and 0.47 eV (tri-interstitials) are lower than 0.98 eV in the single interstitial migration energy case. The migration times can, and will be, converted to diffusivities, which would retain the Arrhenius activation energies but change the pre-exponential factors.

The simulations presented above used the Morelon potential and mostly applied standard MD techniques. The same simulations were unsuccessful for the CRG potential, since the barriers are high enough to grind migration events to a halt on time scales within reach for standard MD. We are currently applying AMD simulations to the CRG potential with promising initial results. Specifically, we ran simulation on 576 cores on one of the LANL HPC platforms for 16 hours with 32 replicas, giving us $\sim 95\%$ parallel efficiency and a simulation times of $\sim 0.5 \mu\text{s}$. This should be a sufficient increase to extract results for the uranium interstitial cluster diffusivities.

Thrust 2: Spatially discretized cluster dynamics and MARMOT phase field simulations to understand fission gas bubble behavior

Effort at ORNL, UTK and UF, with support from the MOOSE team at INL, has been focused on coupling Xolotl and MARMOT through MOOSE, as well as improving the computational performance of Xolotl.

Xolotl Performance and Scalability

In this project, Xolotl is used to model the behavior of fission gas (initially Xe) atoms and clusters (eventually bubbles) in the UO_2 matrix. The code is written in C++ and built around the PETSc solver library (PETSc developers at ANL are also part of this project). Parallelism is supported using MPI. Historically, we have taken a very pragmatic approach to the performance and scalability of Xolotl, identifying and addressing bottlenecks to completing our science goals as the project progresses rather than spending a lot of effort on optimizations that may turn out to be premature. Xolotl is also developed and used in conjunction with the PSI2 FES SciDAC project. Some issues will arise because of the different ways in which the two different types of systems being modeled exercise the code. But in general, most of the performance and scalability issues encountered in one class of applications will eventually impact others. And some issues have broad impact from the start. For example, because the reaction networks for the fission gas case tend to be significantly larger than those for the plasma case, we tend to encounter problems with memory usage in the fission gas context. But the solutions benefit all uses. The team working on Xolotl is jointly supported by both SciDAC partnership projects; additionally, Phil Roth is a member of the RAPIDS SciDAC Institute focusing on application engagement and performance issues.

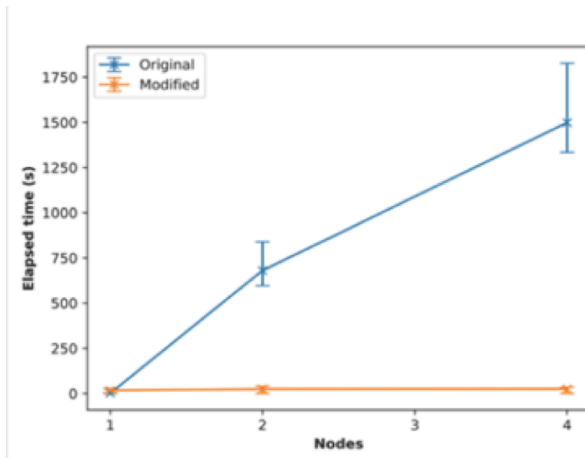


Figure 7. Elapsed time for Xolotl runs before and after I/O code improvements. On OLCF’s Cray XC30 (Eos), 32 processes per node. Performance improvement at 4 nodes (128 processes) is 57.5x.

An example of a recent performance-related activity is shown in Figure 7. As a result of our built-in, always-on performance data collection, we noticed that a routine associated with checkpointing and restarting Xolotl simulations was not scaling as expected. More detailed profiling of the routine revealed that a misunderstanding of the interface for the HDF5 I/O library led every process storing a copy of the entire dataset, rather than each process writing only the portion that it “owned”. Changing the routine to use the true parallel write resulted in a significant improvement in performance, as shown in Fig. 7 (57.5x at 128 processes for one test case) and scalability.

We have also been anticipating the need to adapt the code to take better advantage of GPU accelerators, SIMD vector units, and other on-node hardware features as our simulations grow larger and more complex. Previous experiments have suggested that the Kokkos library would be an effective path forward, providing both the performance and the portability we desire. Kokkos provides abstractions for both parallel execution and memory management which can be mapped effectively onto a variety of programming environment targets, including OpenMP, Pthreads, and CUDA, which in turn support many-core, vector, GPU, and other hardware architectures. The Kokkos library was initially developed by Sandia National Laboratories and is seeing increasing uptake across a broad range of computational science and engineering applications. Development of Kokkos is currently supported primarily by the Exascale Computing Project. We are now in the process of developing a Kokkos-based implementation of the reaction network capabilities of

Xolotl, which we refer to as XNR. We have also discussed with PETSc team members on this project how best to integrate Kokkos more directly with PETSc. They have already completed preliminary work on such an integration, which we will be testing and extending as soon as progress on XNR permits.

Implementation of resolution model into Xolotl

During the past year, we have also implemented the fission gas re-resolution model developed by Setyawan and co-workers [24], which was a significant outcome of the pilot fission gas SciDAC project. Figure 8 shows results of Xolotl predictions of the xenon cluster size distributions as a function of different implementations of the re-resolution model, as well as a function of time. In this simulation, we have assumed a fuel temperature of 1800 K and a fission rate density of 8×10^{19} fissions $\text{m}^{-3} \text{s}^{-1}$, and parametrically varied the minimum xenon cluster size for which heterogeneous resolution occurs. The left side pane in Figure 8, plots the effect of the minimum cluster size at which resolution is implemented according to the Setyawan model at a time of 10^7 seconds, while the right hand pane of Fig. 8 assumes the minimum cluster for which resolution occurs is a 15-member xenon cluster, and plots the size distribution as a function of time. As is evident in Fig. 8 (left), the implementation of the re-resolution model such that all xenon clusters are subject to resolution (min=0, blue curve), results in a significantly larger concentration of xenon monomers and a slight increase in the maximum cluster size. By increasing the minimum size at which resolution begins, there is the beginning hints of a bi-modal size distribution since the peak xenon cluster population occurs for a cluster size of 9 or 14, respectively with re-resolution minimum size of 10 or 15 (red, yellow lines, respectively).

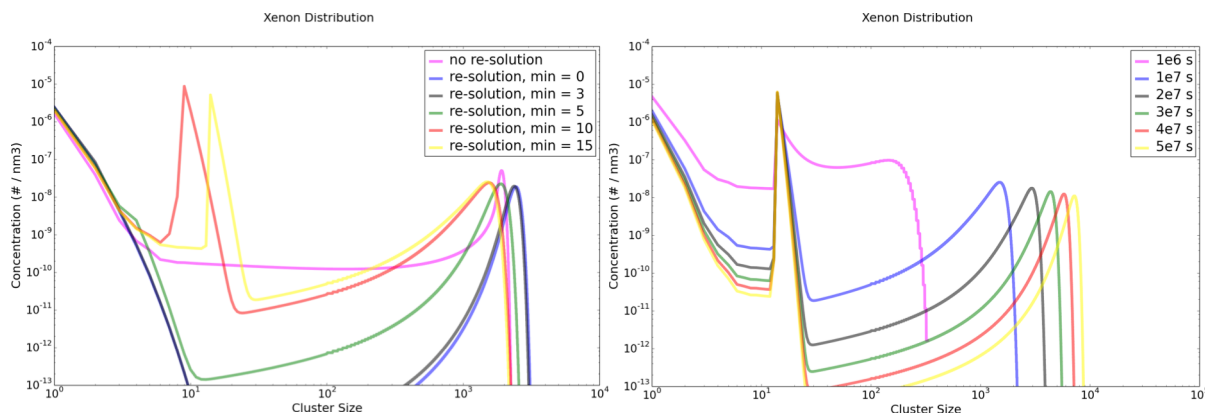


Figure 8. Xolotl predictions of the intragranular xenon cluster concentration as a function of the parametric implementation of the heterogeneous resolution model (left), and as a function of time using a minimum xenon cluster size experiencing resolution of 15 xenon atoms (right).

With increasing time, the size distribution slowly increases the maximum cluster size, but the peak concentration remains at a nearly constant concentration value at the size just below the onset of resolution. The strong size dependent resolution model developed by Setyawan may need to be revised to ensure that the model captures the development of a bi-modal size distribution that is observed experimentally. While this initial study used a minimum cluster size as the onset for heterogeneous resolution, this is not physically valid, and in the future, we will evaluate the influence of the effective electronic stopping, which for smaller values will reduce the size dependence of the resolution rates, as well as the absolute magnitude. However, this initial result does indicate that the numerical model has been implemented correctly in Xolotl.

Xolotl – MARMOT Coupling

Another new activity this year has been the beginning of work on coupling of Xolotl with the MARMOT phase-field code. MARMOT is built on the MOOSE framework, developed primarily at Idaho National Laboratory. Project members at University of Tennessee, University of Florida, and Idaho, Los Alamos, and Oak Ridge National Laboratories have begun meeting regularly to track progress and address issues as we develop this capability. ORNL researchers have contributed to architectural, performance, and debugging discussions as the work has progressed. The team is now at the stage of initial exploratory simulations at a modest scale. As we scale up, we expect to encounter new performance issues in Xolotl individually, MARMOT/MOOSE individually, and in the coupling, which will need to be addressed as they occur.

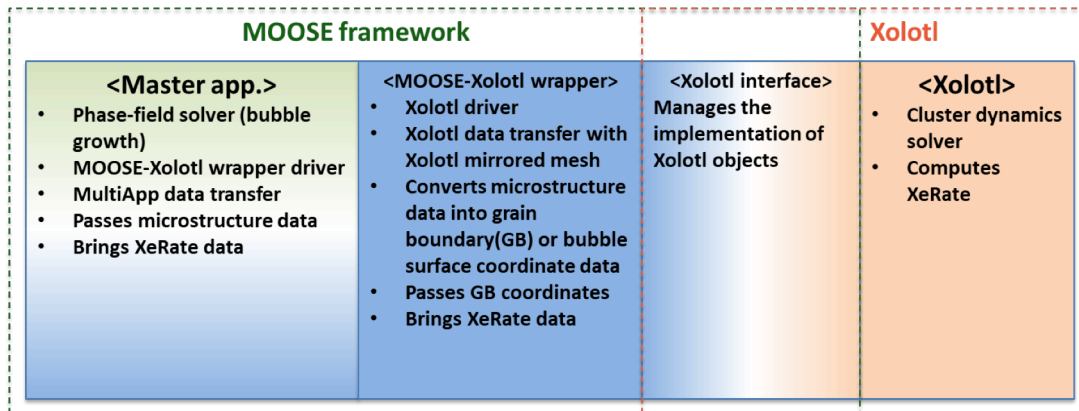


Figure 9. Coupling method schemes showing layered structure of the coupled applications, and the main roles of each.

For the coupling between MARMOT and Xolotl we use the MultiApp capability from MOOSE, since MARMOT is built upon MOOSE. The coupled application is accessible through GitHub [25] along with the coupling version of Xolotl [26], and schematically illustrated in Figure 9. The coupled application employs two-way parallel data transfer to send fission gas flux data from Xolotl to MARMOT and grain boundary location data from MARMOT to Xolotl. The data transfer was managed through the MOOSE-Xolotl wrapper. To send Xolotl fission gas flux data to Master application, MOOSE-Xolotl wrapper directly copies the flux data and saves it in the mirrored meshed MOOSE data. Subsequently, the copied flux data is sent to the Master application, interpolating the data between the different meshes (allowing the use of adaptive meshing in MARMOT). To send the grain boundary locations to Xolotl, microstructure data is sent from the Master application to the MOOSE-Xolotl again using interpolation. The list of grain boundary locations is composed and then sent to Xolotl. This is summarized in Fig. 10.

For external applications like Xolotl, it is necessary to create a wrapper in MOOSE that will call specific methods in Xolotl. The first step was then to create a new interface class in Xolotl implementing methods like initialize(), solve(), and finalize(); and which will be the only class the MOOSE wrapper will need to know about. This step was beneficial to Xolotl as it allowed us to clean up the main() method and directly call the methods from the interface. The next step is to compile Xolotl as a dynamic library instead of only creating the executable, in order for MOOSE to use it as a dependency. We added an option to Xolotl at configure time specifying which type of build is wanted, as a library or as an executable.

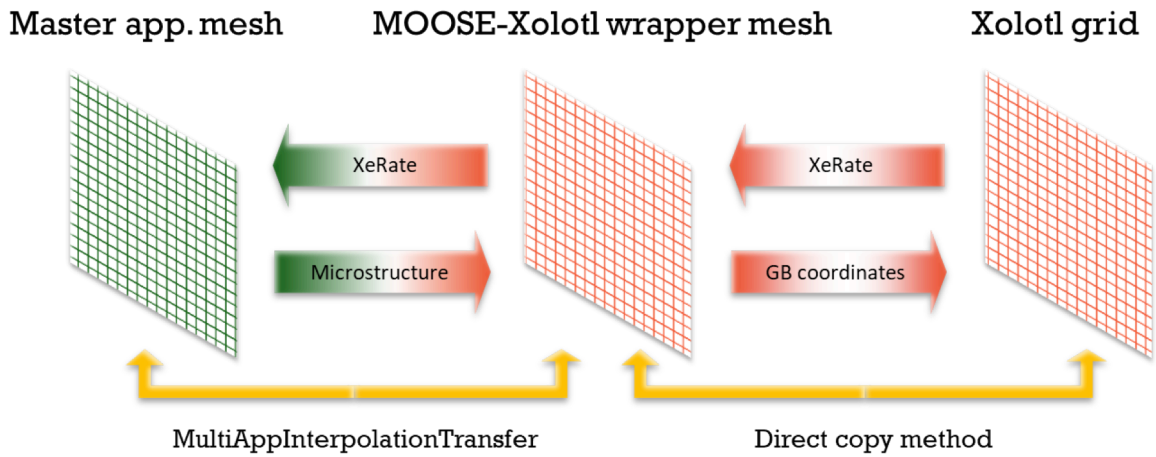


Figure 10. Schematic illustration of data transfer procedure through the MOOSE-Xolotl wrapper.

During the initial tests of the coupled simulation, we realized that some of the PETSc options given in the Xolotl parameter file were not read correctly, while there was no issue when Xolotl was run stand alone. The problem came from the fact that both MOOSE and Xolotl rely on PETSc for their solvers and that a unique pool of options was created, causing some of the MOOSE PETSc options to overwrite the Xolotl PETSc options. We worked with the PETSc team to create a separate options pool in Xolotl that stays separate from the MOOSE one.

In parallel, we prepared Xolotl to accommodate modeling of grain boundaries (GBs). We model them as free surfaces, meaning that there is a zero xenon concentration condition on the grid points where they are located. Xolotl simply takes an input file that lists the locations of the GBs in the grid coordinates to know where to apply the free surface boundary condition. Additionally, we are interested in computing the flux of mobile xenon (Xe) diffusing toward the GBs. This is done at the end of each time step in Xolotl: we loop over all the GBs grid points and add the contribution from diffusion from the neighboring grid points using the finite difference approximation. The implementation of the free surface GBs was

completed in a straight forward manner and not optimized for parallel computation. Initial scaling studies (red dots in Figure 11) indicate that increasing the coverage of the GBs (number of grid points representing a GB divided by total number of grid points) significantly increases the computational cost (wall clock run time) of Xolotl. Optimization of the code in MPI shows an improvement of up to more than an order of magnitude in the simulation time of Xolotl (blue dots in Figure 11).

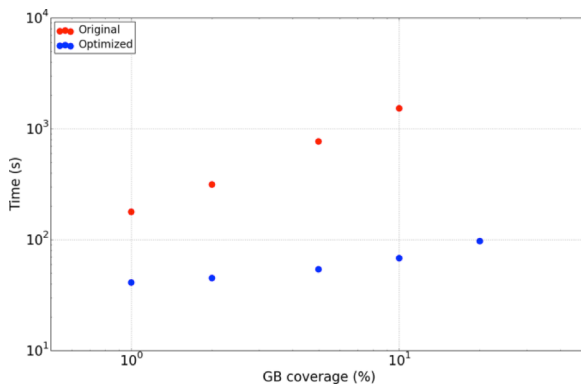


Figure 11. Total simulation time for Xolotl to reach 2×10^5 seconds on a 600×600 finite difference grid, as a function of grain boundary coverage (% of grid points modeled as GBs). The initial implementation in Xolotl is shown in red, while the blue points demonstrate the computational time for an optimized GB implementation.

MOOSE transfer capabilities to exchange them. More specifically, the transfer happens between two meshes: one is the mesh on which the phase field model is performed, the other one is a mesh created by the Xolotl wrapper in MOOSE which mimics the geometry of the grid used in Xolotl, including the way it

is split in parallel to make the transfer between this mesh and the Xolotl data efficient. The two meshes (phase field and from the Xolotl wrapper) do not need to have the same geometry nor resolution. At each loop of the coupled code, the Xolotl wrapper populates its mesh with the local flux computed by Xolotl by calling a method defined in the interface presented at the beginning of this section. These values are then transferred to the phase field model. Similarly, the Xolotl wrapper determines the location of the GBs from the phase field data and generates a list of values that is then passed to Xolotl through its interface before starting again.

As an initial example of the coupled Xolotl-MARMOT simulation, Figure 12 presents the results of an polycrystal simulation of fission gas evolution at 5×10^3 and 4×10^7 seconds. In this initial simulation, xenon clustering was not allowed in Xolotl, in order to maximize the xenon flux to the grain boundary passed to MARMOT. Fig. 12 does demonstrate successful coupling of Xolotl to MARMOT, and thus we can conclude that the two-way data transfer is effective. The fission gas flux data from Xolotl is provided to MARMOT on both sides of the grain boundary, resulting in the buildup of gas on the grain boundaries and triple junctions. These gas atoms cause the growth of the initial bubbles.

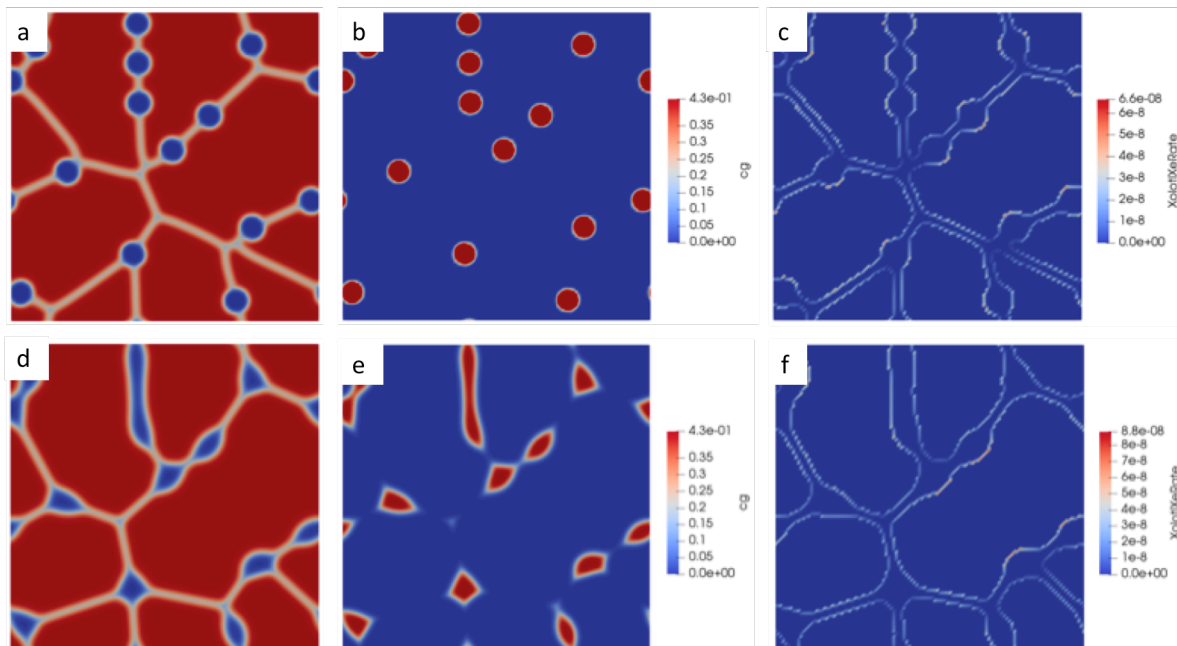


Figure 12. Initial results of coupled MARMOT-Xolotl calculation of fission gas in a polycrystalline UO_2 sample, in which the top frames (a,b,c) are at a time of 5×10^3 seconds, while the bottom panes are at 4×10^7 seconds. The left frames (a,d) show the grain boundary locations and grain boundary bubbles, while the middle panes (b,e) show the fission gas concentrations calculated by MARMOT, and the right panes (c,f) show the Xolotl calculated xenon flux to the grain boundary. It is important to note that intragranular xenon clustering and bubble formation was not included in the current simulations.

Enhancement of fission gas bubble model in MARMOT

In MARMOT, we are using the most up-to-date fission gas model available in the code [27]. In order to optimize the fission gas model, it is critical that the MARMOT simulations run efficiently. For that reason, we have analyzed the impact of various solution parameters on the wall time. In all cases, PETSc was used to solve the system with preconditioned Jacobian-Free Newton-Krylov using the Additive Schwarz method (ASM). With ASM, we explored the impact of using ILU or LU decomposition in the sub-blocks, using a linear predictor with the solve, and using the additional PETSc options of `pc_asm_overlap = 1` and `pc_factor_levels = 2`. The simulations were carried out on a MacPro with a ten core 3 GHz processor using all ten cores. The results are shown in Fig. 13. From this study, we found that

using LU with the predictor block and the two additional PETSc options resulted in the lowest wall time by a factor of six. This speedup was due to improved convergence allowing larger time steps to be taken.

In addition to the numerical performance of the simulations, we have also been making major improvements on making physically representative simulations that are using the best available parameters for UO_2 for the vacancy and gas mobility, as well as the grain boundary migration and grain boundary energy. We have obtained the best parameters using a combination of atomic-scale simulations and taking experimental data from the literature.

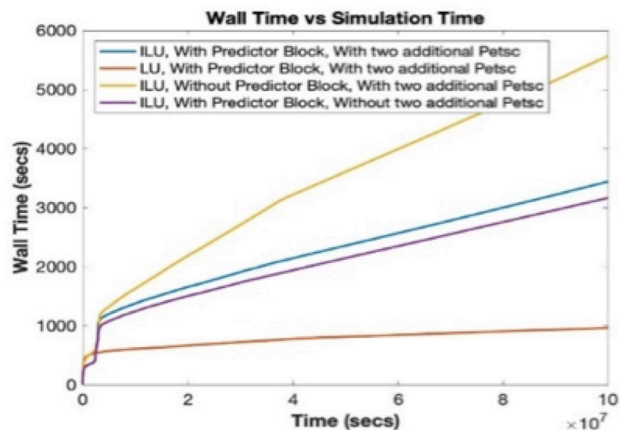


Figure 13. Wall time improvement of MARMOT fission gas simulations by changing solution options.

Thrust 3: Uncertainty quantification and experimental validation

Engineering scale modeling and experimental validation

The engineering-scale development effort at INL aims to develop improved models for intra-granular fission gas bubble evolution and gas diffusion to be applied in fuel performance codes such as Bison. During FY-17 and FY-18, we developed a reduced parameter model for the evolution of intra-granular fission gas bubbles coupled to diffusion of gas atoms to grain boundaries during normal operating reactor conditions. Details are given in the FY-18 INL milestone report [28] and in publications related to this work [29-31].

During FY-19, the bulk of the work performed to date at INL was devoted to developing an extended fission gas bubble evolution model that is able to capture transient behavior. In particular, the model was extended to account for the so-called bubble coarsening and the associated fuel swelling during transients. This generalization required in the first place the development of a reliable theory for the coarsening mechanisms. Then, a reduced parameter approach for application to engineering codes was developed. Furthermore, early validation to experimental data of bubble sizes in transient-tested fuel was performed. In addition to this, during FY-19, the original normal operation model was further developed by coupling to atomistic calculations for gas atom diffusivity in Cr_2O_3 doped UO_2 performed at LANL. The enhanced model was applied in Bison fuel rod simulations, demonstrating the impact of the multiscale coupling. These FY-19 developments and applications of the engineering fission gas model are presented below.

New model for intra-granular bubble evolution during transients

During normal operating conditions, intra-granular fission gas bubbles generally have diameters of one to a few nanometers. However, experiments have shown that during transient conditions such as power ramps, a strongly bi-modal bubble size distribution develops, with the appearance of a second population of coarsened bubbles with diameters of tens to hundreds of nm [11-13,32]. Bubble coarsening is associated with large local gaseous swelling during transients [11,13] and is therefore of high engineering importance. Recent research at INL within this SciDAC project has led to the development of a bubble coarsening theory that invokes the role of dislocations as a source of vacancies and preferential bubble growth along dislocations. This theory finds support in the experimental observations showing coarsened bubbles associated with dislocations (e.g., [12,13]). It also appears to be a straightforward conceptual extension to dislocation defects of the established behavior at grain boundary defects.

The newly developed transient model extends the normal operating conditions model developed in previous years by adding the evolution of a second population of bubbles along dislocations, which is subject to coarsening. The coarsening mechanism is naturally activated during transient conditions according to the physical representation in the model. While both small bubbles in the bulk and coarsening bubbles at dislocations are modeled, only the average size of each population is considered. In the following, we provide a brief summary of the model, leaving a detailed description and expressions for the parameters to a future publication. The governing equations in the model's final form are:

$$\begin{aligned}
\frac{\partial N_b}{\partial t} &= \nu - \alpha_{\bar{n}_b} N_b \\
\frac{\partial N_d}{\partial t} &= z \frac{\partial \rho_d}{\partial t} - \alpha_{\bar{n}_d} N_d \\
\frac{\partial m_b}{\partial t} &= 2\nu + \beta_{\bar{n}_b} N_b - \alpha_{\bar{n}_b} m_b \\
\frac{\partial m_d}{\partial t} &= \beta' c_1 + \beta_{\bar{n}_d} N_d - \alpha_{\bar{n}_d} m_d \\
\frac{\partial c_1}{\partial t} &= \gamma F + D \nabla^2 c_1 - 2\nu - \beta_{\bar{n}_b} N_b + \alpha_{\bar{n}_b} m_b - \beta' c_1 - \beta_{\bar{n}_d} N_d + \alpha_{\bar{n}_d} m_d
\end{aligned} \tag{1}$$

where t is the time, N_b and N_d (m^{-3}) the number densities of bubbles in the bulk and at dislocations, respectively, m_b and m_d (m^{-3}) the concentrations of gas atoms in bubbles, $\bar{n}_b = m_b/N_b$ and $\bar{n}_d = m_d/N_d$ (-) the average numbers of gas atoms per bubble, c_1 (m^{-3}) the concentration of single gas atoms, ν ($\text{m}^{-3}\text{s}^{-1}$) the rate of bubble nucleation in the bulk, β_n (s^{-1}) the rate of gas atom trapping at bubbles of size n , β' (s^{-1}) the trapping rate at dislocations, α_n (s^{-1}) the re-solution rate from bubbles of size n , z (m^{-1}) a constant, ρ_d (m^{-2}) the dislocation density, γ (/) the yield of fission gas atoms, F ($\text{m}^{-3}\text{s}^{-1}$) the fission rate density, D (m^2s^{-1}) the diffusion coefficient of single gas atoms.

The solution of Eq. 1 provides the rate of single gas atom diffusion to grain boundaries, the number density of both bubbles in the bulk and at dislocations, and the average number of atoms per bubble. The radius of bubbles in the bulk is calculated considering a constant gas density as [28-30]

$$R_b = B \bar{n}_b^{-1/3} \tag{2}$$

For bubbles at dislocations, vacancy absorption is considered using the following model:

$$\frac{\partial \bar{n}_v}{\partial t} = \frac{2\pi D_{v,pipe} b}{kTs} \left(\frac{kT \bar{n}_d}{\Omega \bar{n}_v} - p_{eq} \right) \tag{3}$$

where \bar{n}_v (-) is the number of vacancies per bubble, $D_{v,pipe}$ (m^2s^{-1}) the pipe diffusion coefficient of vacancies along dislocations, $b = (3/4\pi N_d)^{1/3}$ the radius of the Wigner-Seitz cell associated with a bubble at a dislocation, k (JK^{-1}) the Boltzmann constant, s (-) a geometric factor, and p_{eq} (Pa) the bubble equilibrium pressure given by the sum of the surface tension and hydrostatic stress. The first term in brackets represents the bubble internal energy, so that vacancy absorption is activated once the internal energy exceeds the equilibrium pressure. This condition is naturally met during temperature increases such as reactor transients to high power. The radius of bubbles at dislocations is calculated as

$$R_d = \left(\frac{3}{4\pi} \right)^{1/3} (\omega \bar{n}_d + \Omega \bar{n}_v)^{1/3} \tag{4}$$

where ω (m^3) is the van der Waals volume of a fission gas atom and Ω (m^3) is the vacancy volume. The model also considers bubble coalescence, although details are not given here for brevity.

Fig. 14 shows the early validation results of the extended model to experimental data for the size of coarsened bubbles along dislocations from SEM observations on various power ramped UO_2 fuel samples in [12]. Results demonstrate that the extended model is able to represent the appearance of bubbles with radii of tens to hundreds of nm during transients. Note that traditional models applied in current engineering codes neglect this effect and only predict bubble sizes of up to a few nm. It follows that the new model introduces the potential to accurately compute the large gaseous swelling due to intra-granular bubbles during transients. To the best of our knowledge, this is a first-time development of a physically based bubble coarsening model applied in engineering calculations.

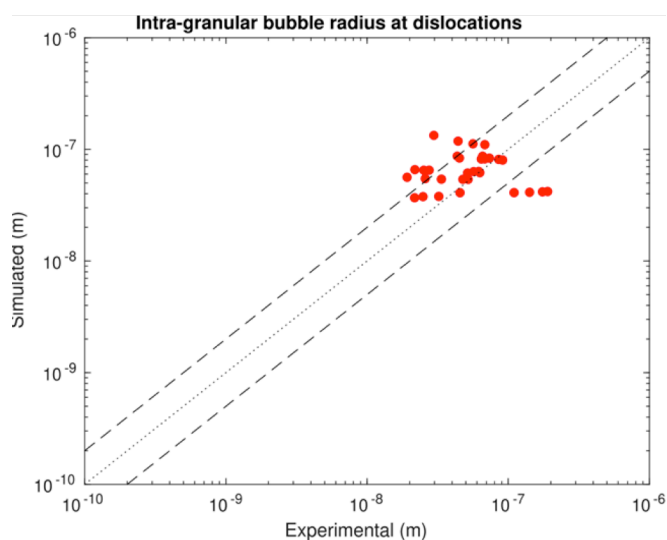


Figure 14. Comparison of predicted to measured radii of coarsened intragranular bubbles from power ramp experiments [12].

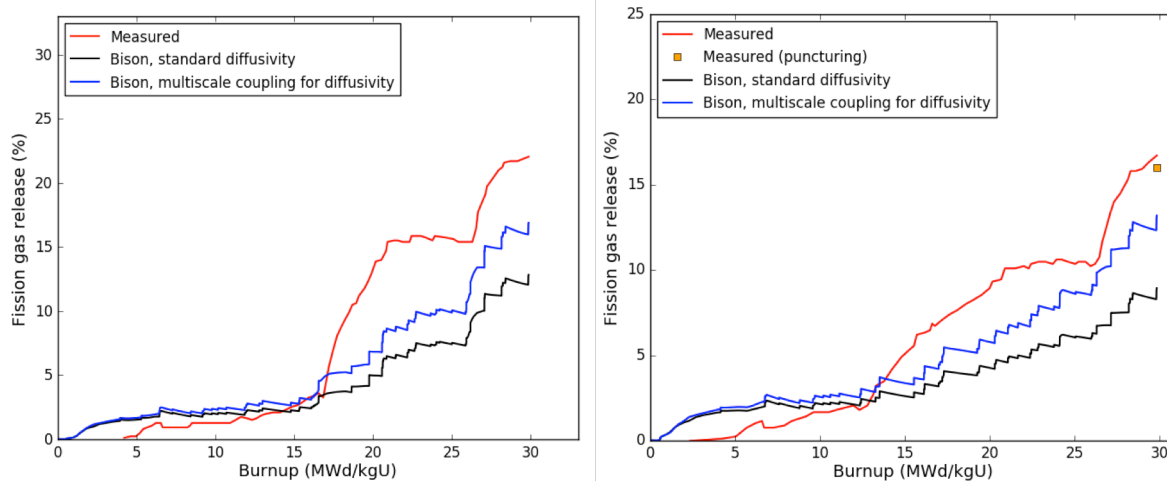


Figure 15. Comparisons of predicted to measured fission gas release for the Halden tests IFA-677.1 rod 1 (left) and rod 5 (right). Calculations were performed with the Bison code.

For the base model for normal operating conditions, model development and validation to separate-effects experimental data are presented in [28,30], and applications to integral fuel rod simulations with Bison are presented in [29]. During FY-19, the model was coupled to lower-length scale calculations for fission gas atom diffusivity in Cr_2O_3 doped UO_2 from LANL [32] and applied to integral fuel rod calculations with Bison. In particular, Cr_2O_3 -doped UO_2 fuel rods from the Halden test IFA-677 [34] were simulated. Fig. 15 shows the comparisons of integral FGR predictions from the Bison calculations to the experimental data. Results demonstrate the good overall agreement obtained using the new intra-granular fission gas model, as well as the further improvement obtained with the multiscale coupling to the atomistic model for diffusivity. This work on Cr_2O_3 -doped UO_2 modeling at INL was co-funded by SciDAC and CASL.

Uncertainty Quantification

The uncertainty quantification effort has concentrated on performing sensitivity analysis of computer codes, specifically the Free Energy Cluster Dynamics (FECD) solver and the Xolotl code. Sensitivity analysis is necessary to identify active input parameters that influence output quantities of interest, such that efficient surrogate models can be built using these active parameters to ultimately replace the expensive computations associated with these solvers when performing uncertainty propagation to discover distributions on these quantities of interest. We are interested in performing global sensitivity analysis specifically in order to take into account potential correlated behavior between parameters with respect to their impact on the quantities of interest (QoI).

In the FECD case, an initial effort to compute the fractional variance contribution of each input parameter to the QoIs, i.e. Sobol sensitivity indices, used approximately 10,000 samples of the FECD code. These 10,000 samples were then used to estimate integrals using Monte Carlo estimation to compute the sensitivity indices. One particular challenge that arose in this effort is that different combinations of the parameters resulted in run failures. Because the sampling strategy used to compute the integrals relies implicitly on the information from these runs being available, the effective number of samples is then drastically reduced. The computation of sensitivity indices with this subset of samples revealed approximately 15-20 dominant parameters (see Fig. 16).

In order to overstep the issue of failed runs with regards to increasing the number of effective samples used to estimate the sensitivity indices, we moved to a framework of estimating the sensitivity indices using polynomial chaos expansion (PCE) constructions where the sensitivity indices are easily extractable from the expansion coefficients. First, an effort was performed to reevaluate the form of input uncertainties themselves. In the earlier effort, the nominal values and bounds on the parameters were used to define uniform sampling densities on intervals. This

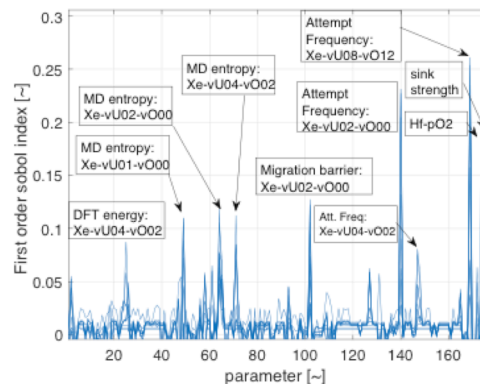


Figure 16. Sensitivity indices for FECD QoIs.

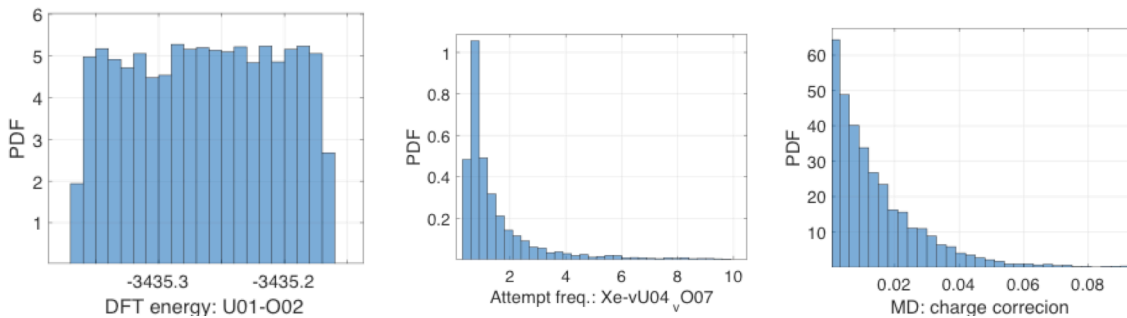


Figure 17. Uniform, log-normal, and exponential distributions used in the updated sampling strategy.

construction is hypothesized to cause issues when samples are drawn from the corners of the sample space, which may be causing extreme parameter combinations that may result in failures. When nominal parameters are defined with values closer to one bound, log-normal distributions are assumed. When a nominal value is specified to be equal to the value of one bound, exponential distributions are assumed. This construction was envisaged to result in fewer samples resulting in extreme parameter values by

clustering probability near the nominal values. Figure 17 shows examples of the new distributions employed.

We employed a Bayesian inference strategy to estimate the PCE coefficients and ultimately the main and total sensitivity indices. The total sensitivity indices take into account both the individual fraction contributions of each parameter to the QoI variance as well as any contribution due to joint variation. Of particular interest is the determination of the number of samples required to make accurately converged estimates of the PCE coefficients and resulting sensitivity indices. We start by assuming 20 active parameters (see Fig. 178).

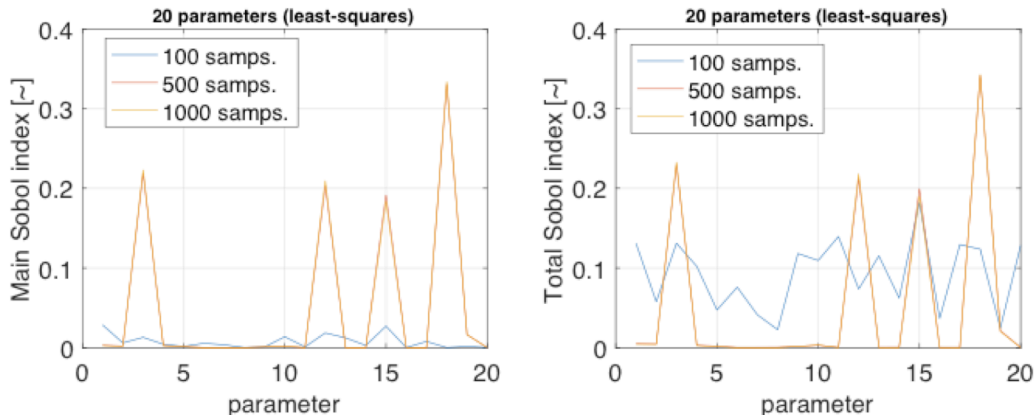


Figure 18. Sensitivity indices estimated using Bayesian-PCE fitting, considering 20 parameters, where 4 active parameters are identified.

This effort identified four parameters that dominate the contribution to the QoI variance, with well converged estimates when using more than 500 samples. These computations also demonstrated that many of the PCE coefficients are close to zero. As such, a strategy for estimating the coefficients using algorithms that aim to explicitly identify sparsity, particularly Bayesian compressive sensing (BCS), were employed. Figure 19 shows a re-computation of the results in Fig. 18 where the sparsity is identified, even for a smaller number of samples (100).

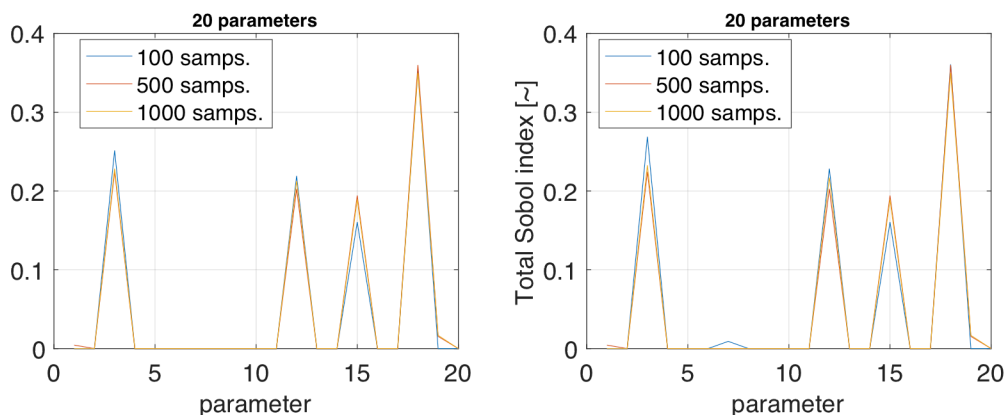


Figure 19. Sensitivity indices estimated using BCS-PCE fitting, considering 20 parameters, where 4 active parameters are identified.

The computations were then performed for increasing numbers of parameters (see Figs. 20 and 21) ultimately expanding to the full parameter set, showing that, for the full parameter set, a consistent set of 12 parameters is identified once more than 1000 samples are used, even if the convergence of the

estimated indices may require more than 4000 samples. Further sampling will be performed to test this convergence.

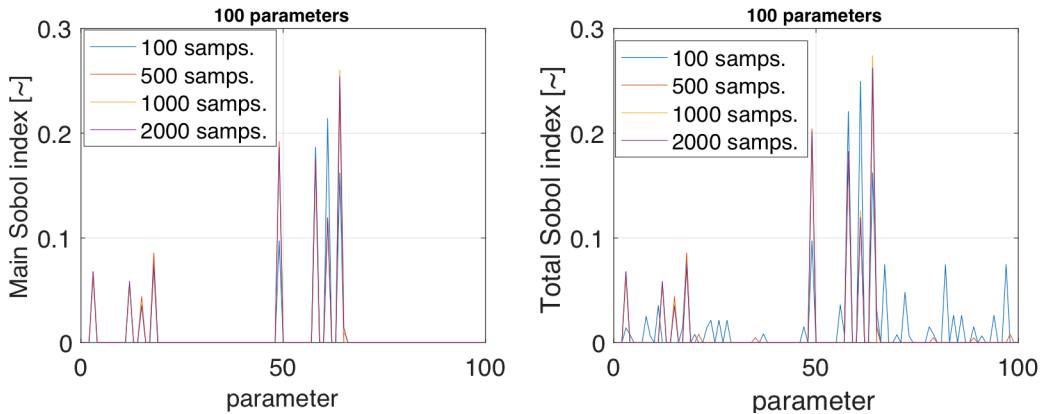


Figure 20. Sensitivity indices estimated using BCS-PCE, considering 100 parameters, where 8 active parameters were identified.

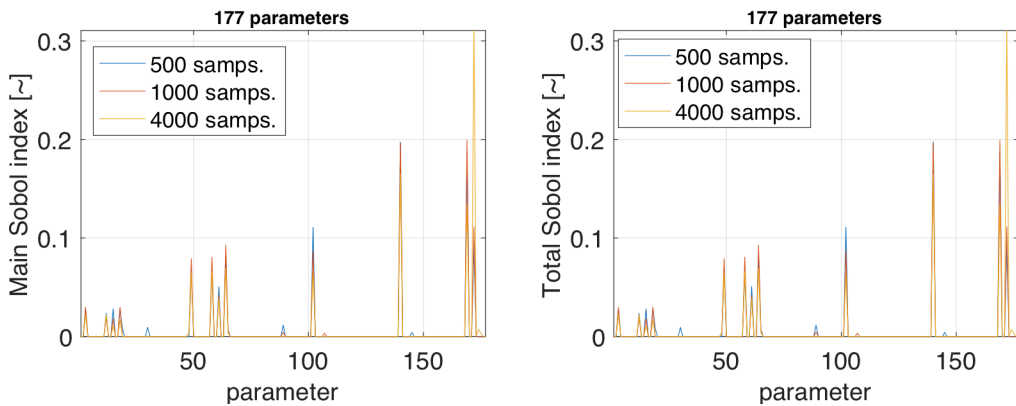


Figure 21. Sensitivity indices estimated using BCS-PCE, considering 1770 parameters, where 12 active parameters were identified.

Overall, the new framework of using the updated density constructions resulted in a failure rate of approximately 4%, while the BCS-PCE approach identified 12 active parameters when computing PCEs. The resulting 12-dimensional PCEs can now be used to propagate uncertainty to estimate distributions on the QoIs. This effort is ongoing. Ultimately this surrogate will be used in concert with available experimental data to perform Bayesian parameter estimation on a particular input parameter which has been identified as a useful tuning parameter, and whose nominal value and uncertainty bounds are essentially notional.

Global sensitive analysis was also applied to the Xolotl code. Xolotl is a significantly more expensive model than FECD, with each run requiring hours of multiple node computation, and 1000 runs were performed to make an initial rough estimate of the sensitivity indices. Two dominant parameters were identified, but further analysis is required to establish the convergence of these estimates, and thus arrive at reliable values.

Further work will focus on constructing the FECD surrogate for the small subset of active parameters and constructing the Bayesian parameter estimation problem for the tuning parameter using available experimental data. Convergence of the sensitivity estimates for Xolotl will also be considered, in particular with relation to eventual FECD-Xolotl coupling.

SUMMARY

This document describes the project progress in the second year, from approximately June 2018 – May 2019. Our most significant outcomes have involved development of the coupling framework for Xolotl and MARMOT, continued performance improvements in Xolotl, uncertainty quantification analysis of the free energy cluster dynamics and Xolotl codes, new engineering scale model for intra-granular bubble evolution during transients, and to finalize the Xe diffusion model based on extended vacancy clusters. Plans for the coming year include refining the fission gas resolution model implemented in Xolotl by benchmarking to a wide range of experimental datasets, implementing a 2-dimensional (Xenon-vacancy) phase space to describe the xenon diffusion and clustering evolution that will enable us to predict the evolution of the xenon density (pressure) in fission gas bubbles, along with extending the UQ efforts to Xolotl, and to continuing the development of the coupled Xolotl-MARMOT simulations to 3-dimensions with fully representative physics to enable experimental validation.

BIBLIOGRAPHY

Presentations:

- B.D. Wirth, D. Andersson, S. Blondel, M. Cooper, and W. Setyawan, on behalf of NE SciDAC Pilot and Fission Gas SciDAC team, invited talk at 2018 Spring MRS Meeting, "[Multiscale Modeling of Fission Gas Bubble Evolution in UO₂ Under Normal Operating Conditions](#)", 3 April 2018
- B.D. Wirth, on behalf of NE SciDAC Pilot and Fission Gas SciDAC team, overview of NE SciDAC project to the ASCR FastMath and Rapids Institutes, "[Simulation of fission gas in Uranium Oxide Nuclear Fuel](#)", 16 April 2018
- G. Pastore, D.A. Andersson, C.R. Stanek, W. Setyawan, R.J. Kurtz, B.D. Wirth, et al., "[Multiscale Modeling of Fission Gas Behavior for BISON](#)" OECD/NEA 14th meeting of the Working Party on Multiscale Modelling of Fuels and Structural Materials for Nuclear Systems (WPMM), Paris, France, May 15-17, 2018
- B.D. Wirth, D. Andersson, S. Blondel, M. Cooper, and W. Setyawan, "[Mutiscale Modeling of Fission Gas Bubble Evolution in UO₂ under Nominal Operating Conditions](#)", 2018 Nuclear Materials Conference (NuMat), Seattle, WA, 15 October 2018

Publications:

- T. D. Swinburne and D. Perez, "[Self-optimized construction of transition rate matrices from accelerated atomistic simulations with Bayesian uncertainty quantification](#)", Physical Review Materials, May 2018. doi: 10.1103/PhysRevMaterials.2.053802
- G. Pastore, D. Pizzocri, C. Rabiti, T. Barani, P. Van Uffelen, L. Luzzi, "An effective numerical algorithm for intra-granular fission gas release during non-equilibrium trapping and resolution". Journal of Nuclear Materials 509, 687, 2018. <https://doi.org/10.1016/j.jnucmat.2018.07.030>
- W. Setyawan, M.W.D. Cooper, K.J. Roche, R.J. Kurtz, B.P. Uberuaga, D.A. Andersson, and B.D. Wirth, "[Atomistic Model of Xenon Gas Bubble Re-resolution Rate due to Thermal Spike in Uranium Oxide](#)", *Journal of Applied Physics* **124** (2018) 075107
- Perriot, C. Matthews, M. W. D. Cooper, B. P. Uberuaga, C. R. Stanek, D. A. Andersson, "Atomistic modeling of out-of-pile xenon diffusion by vacancy clusters in UO₂". J. Nuclear. Mater. 520, 96 (2019).

REFERENCES

- [1]. D.R. Olander, Fundamental Aspects of Nuclear Reactor Fuel Elements, TID-26711-P1, National Technical Information Services (1976).
- [2]. G. Pastore, L. Luzzi, V. Di Marcello, P. van Uffelen, “Physics-based modelling of fission gas swelling and release in UO₂ applied to integral fuel rod analysis”, *Nuclear Engineering and Design* **256** (2013) 75.
- [3]. A.H. Booth, “A method of calculating fission gas diffusion from UO₂ fuel and its application to the X-2-f loop test”, Canadian Report CRDC-721, September 1957.
- [4]. M.V. Speight, “A Calculation on migration of fission gas in material exhibiting precipitation and resolution of gas atoms under irradiation”, *Nuclear Science & Engineering* **37** (1969) 180.
- [5]. R.M. Cornell, M.V. Speight and B.C. Masters, “Role of bubbles in fission gas release from uranium dioxide”, *Journal of Nuclear Materials* **30** (1969) 170-178.
- [6]. J.A. Turnbull, C.A. Friskney, J.R. Findlay, F.A. Johnson, and A.J. Walter, “The diffusion-coefficients of gaseous and volatile species during the irradiation of uranium-dioxide”, *Journal of Nuclear Materials* **107** (1982) 168-184.
- [7]. R.J. White and M.O. Tucker, “A new fission-gas release model”, *Journal of Nuclear Materials* **118** (1983) 1-38.
- [8]. K. Forsberg and A.R. Massih, “Diffusion-theory of fission-gas migration in irradiated nuclear-fuel UO₂”, *Journal of Nuclear Materials* **135** (1985) 140-148.
- [9]. A.R. Massih and K. Forsberg, “Calculation of grain boundary gaseous swelling in UO₂”, *Journal of Nuclear Materials* **377** (2008) 406-408.
- [10]. R.J. White, “The development of grain-face porosity in irradiated oxide fuel”, *Journal of Nuclear Materials* **325** (2004) 61.
- [11]. S. Kashibe, K. Une and K. Nogita, “Formation and growth of intragranular fission-gas bubbles in UO₂ fuels with burnup of 6-83 Gwd/T”, *Journal of Nuclear Materials* **206** (1993) 22-34.
- [12]. R.J. White, R.C. Corcoran and J.P. Barnes, “A Summary of Swelling Data Obtained from the AGR/Halden Ramp Test Programme”, Report R&T/NG/EXT/REP/0206/02 (2006)
- [13]. C. Baker, “Fission-gas bubble distribution in uranium-dioxide from high-temperature irradiated SGHWR fuel pins”, *Journal of Nuclear Materials* **66** (1977) 283-291.
- [14]. P. Lösson, “On the behaviour of intragranular fission gas in UO₂ fuel”, *Journal of Nuclear Materials* **280** (2000) 56-72.
- [15]. Romain Perriot, Christopher Matthews, Michael W.D. Cooper, Blas P. Uberuaga, Christopher R. Stanek, David A. Andersson, Atomistic modeling of out-of-pile xenon diffusion by vacancy clusters in UO₂, *J. Nucl. Mater.* 520 (2019) 96-109.
- [16]. Christopher Matthews, Romain Perriot, Michael Cooper, Christopher R. Stanek, David A. Andersson, “Cluster Dynamics Simulation of Uranium Self-diffusion During Irradiation in UO₂”, submitted (2019).
- [17]. Christopher Matthews, Romain Perriot, Michael Cooper, Christopher R. Stanek, David A. Andersson, “Cluster Dynamics Simulation of Xenon Diffusion During Irradiation in UO₂”, submitted (2019).
- [18]. N.-D. Morelon, D. Ghaleb, J.-M. Delaye, L. Brützel, *Philos Mag* 83 (2003) 1533-1550.
- [19]. M. W. D. Cooper, M. J. D. Rushton, R. W. Grimes, *J. Phys. Condens. Matter.* 26 (2014) 105401.
- [20]. A. Chartier, L. V. Brützel, C. Sabathier, O. Dorosh, J. Jagielski, *Appl. Phys. Lett.* 109 (2016) 181902.
- [21]. A. Voter, *Phys. Rev. B* 57 (1998) R13985.
- [22]. D. Perez, B. Uberuaga, A. Voter, *Comput. Mater. Sci.* 100 (2015) 90.
- [23]. S. Plimpton, *Journal of Computational Physics* 117 (1995) 1-19.

- [24]. W. Setyawan, M.W.D. Cooper, K.J. Roche, R.J. Kurtz, B.P. Uberuaga, D.A. Andersson, B.D. Wirth, Atomistic model of xenon gas bubble re-resolution rate due to thermal spike in uranium oxide, *J. Appl. Phys.* 124, 075107, 2018.
- [25]. https://github.com/eastglow-zz/coupling_xolotl
- [26]. <https://github.com/ORNL-Fusion/xolotl/tree/mooseApps-coupling>
- [27]. L. K. Aegesen, D. Schwen, M. R. Tonks, Y. Zhang, Phase-field modeling of fission gas bubble growth on grain boundaries and triple junctions in UO₂ nuclear fuel, *Computational Materials Science*, **161** (2019) 35-45.
- [28]. G. Pastore, M3MS-18IN0101092: Develop and implement in the BISON code a new engineering model for intra-granular fission gas behavior in uranium dioxide, Tech. Rep. INL/EXT-18-51614, Idaho National Laboratory, USA, September 2018.
- [29]. G. Pastore, T. Barani, D. Pizzocri, A. Magni, L. Luzzi, Modeling fission gas release and bubble evolution in UO₂ for engineering fuel rod analysis, Proc. of Top Fuel 2018, Prague, Czech Republic, 30 September – 4 October 2018.
- [30]. D. Pizzocri, G. Pastore, T. Barani, A. Magni, L. Luzzi, P. Van Uffelen, S.A. Pitts, A. Alfonsi, J.D. Hales, A model describing intra-granular fission gas behaviour in oxide fuel for advanced engineering tools, *J. Nucl. Mater.* 502, 323-330, 2018.
- [31]. G. Pastore, D. Pizzocri, C. Rabiti, T. Barani, P. Van Uffelen, L. Luzzi, An effective numerical algorithm for intra-granular fission gas release during non-equilibrium trapping and resolution, *J. Nucl. Mater.* 509, 687-699, 2018.
- [32]. M. Mogensen, C.T. Walker, I.L.F. Ray, M. Coquerelle, Local fission gas release and swelling in water reactor fuel during slow power transients, *J. Nucl. Mater.* 131, 162-171, 1985.
- [33]. M.W.D. Cooper, C.R. Stanek, D.A. Andersson, The Role of Dopant Charge State on Defect Chemistry and Grain Growth of Doped UO₂, TMS 2019, San Antonio, USA, March 10-14, 2019.
- [34]. H.K. Jenssen, PIE Report on Six UO₂ Fuel Rods Irradiated in IFA-677 High Initial Rating Test, Tech. Rep. HWR-968, OECD Halden Reactor Project, March 2010.